Hybrid organic-inorganic nanoparticles: controlled incorporation of gold nanoparticles into virus-like particles and application in surface-enhanced Raman spectroscopy

Marcus Niebert[*a], James Riches[b], Mark Howes[b], Charles Ferguson[b], Robert G Parton[b], Anton PJ Middelberg[a], Llew Rintoul[c], Peter M Fredericks[c]

[a]Centre for Biomolecular Engineering and Australian Institute for Biomolecular Engineering and Nanotechnology,
[b]Centre for Microscopy and Microanalysis and Institute for Molecular Bioscience
[c]Faculty of Science and School of Physical & Chemical Sciences, Queensland University of Technology

ABSTRACT

A capsid is the protein coat surrounding a virus' genome that ensures its protection and transport. The capsid of murine polyomavirus (muPy) consists of one major (VP1) and two minor (VP2/3) proteins, from which just VP1 is sufficient to form the capsid when expressed recombinantly (1). From a material engineering point of view, viral capsids are of interest because they present a paradigm for complex self-assembly on the nanometer scale. Understanding and controlling these assembly dynamics will allow the construction of nanoscale structures using a self-assembly process. The first step in this direction was the discovery that capsids of several viruses can be reversibly disassembled into their building blocks and reassembled using the same building blocks by simply changing the buffer conditions (2, 3). Such capsids already find applications as targeted *in vivo* delivery vectors for genes, proteins or small molecular drugs (4, 5), as optical probes for biomedical imaging and sensing purposes with unprecedented resolution and sensitivity and can potentially be used as templates for nanoelectronics (6, 7).
Here we show the controlled incorporation of inorganic gold nanoparticles into the capsid shell of muPy. This incorporation is mediated by covalent sulfide bonds between the capsid proteins cysteine residues and the molecular gold. The number of incorporated gold particles can be controlled during the assembly process and the capsids retain their ability to transduce cells. These particles provide new tools for tracking of viral particles in cells, and simultaneously allow the delivery of genes packages in the hollow capsid.

Keywords: virus-like particles, self-assembly, surface enhanced Raman spectroscopy, intracellular trafficking, electron microscopy

1. INTRODUCTION

1.1. Murine polyomavirus

The murine polyomavirus (muPy) is a small, non-enveloped virus with a double-stranded DNA genome of 5kb (8). The viral proteins can be recombinantly expressed in a variety of systems (bacteria (1), yeast [(9) and insect (10) or mammalian cells (11)), where they either form a capsid *in vivo* or the proteins can be assembled to a capsid *in vitro*. A capsid is the protein coat surrounding a virus' genome that ensures its protection and transport. The capsid of murine polyomavirus (muPy) consists of one major (VP1) and two minor (VP2/3) proteins, from which just VP1 is sufficient to form the capsid. The muPy capsid is stabilized by divalent Calcium cations and disulfide bonds (12) and can be disassembled by removing the Ca^{2+}-ions with EGTA and reducing the disulfide bonds by DTT, while reassembly can be initiated by addition of Ca^{2+}-ions and removal of the reducing agent. From a material engineering point of view, viral capsids are of interest because they present a paradigm for complex self-assembly on the nanometer scale. Understanding and

Smart Materials IV, edited by Nicolas H. Voelcker, Proc. of SPIE Vol. 6413, 64130F, (2006)
0277-786X/06/$15 · doi: 10.1117/12.695578

controlling these assembly dynamics will allow the construction of nanoscale structures using a self-assembly process. The first step in this direction was the discovery that capsids of several viruses can be reversibly disassembled into their building blocks and reassembled using the same building blocks by simply changing the buffer conditions. Such capsids already find applications as targeted *in vivo* delivery vectors for genes, proteins or small molecular drugs, as optical probes for biomedical imaging and sensing purposes with unprecedented resolution and sensitivity and can potentially be used as templates for nanoelectronics.
The recombinant production of VP1 protein with subsequent *in vitro* assembly allows a contamination-free process route and makes VLPs an interesting option for gene therapy vectors or for vaccination (13). Reports in the literature showed the packaging of DNA (PCR fragments and plasmids, (4) and small molecular drugs (14)).

1.2. Nanostructural self-assembly

Two complementary strategies can be used to build new molecular biomaterials. In the "top-down" approach, complex structures are broken down to more simple building blocks. In contrast, the "bottom-up" approach assembles complex structures molecule by molecule (15). Molecular self-assembly is mediated by weak, non-covalent bonds – hydrogen, ionic and hydrogen bonds as well as hydrophobic and van-der-Waals interactions. By observing how macromolecular assemblies are governed in nature, we can exploit these processes to built new synthetic materials. Viruses exemplify the paradigm of "bottom-up" nanostructural self-assembly. From a material-engineering point of view, virus-based materials have already been utilized to construct nanofibers (7), batteries (6) and computer memory (16). In addition, viruses have showed great potential in medical application for vaccination (17) and gene therapy (18). Last but not least, gaining knowledge about viral disassembly, especially in the *in vivo* situation, can gain valuable insights for future antiviral therapies or cell biology.

1.3. Surface-enhanced Raman spectroscopy

The Raman spectrum of a typical protein molecule consists of about 30 well-resolved bands in the interval of 500-1750 cm^{-1} and a smaller number of bands between 2500-3500 cm^{-1} mainly characterizing the stretching and bending of the protein main chain. The most prominent bands are amide I and amide III, as well as the sulfhydryl (S-H) stretching vibration of the cysteinyl side chain which occurs uniquely within the narrow range of 2530-2590 cm^{-1} (19). The molecular normal modes of vibration provide a sensitive and selective fingerprint of three-dimensional structure as well as intra- and intermolecular interactions and dynamics. Time-resolved Raman spectroscopy therefore seems to be the ideal tool to elucidate the assembly pathway as well as structural intermediates in icosahedral viruses.
While the assembly of some bacteriophages has been probed by Raman spectroscopy (20-25), this technology has not yet been employed in the characterization of viral parasites of mammals. This is probably due to the fact that these viruses are difficult to obtain in the quantities required for Raman spectroscopy, while bacteriophages can easily be obtained in quantities of several hundred milligrams. To increase the sensitivity of Raman spectroscopy, one can take advantage of surface-enhancement by the presence of nanometer-sized metal particles, mostly silver or gold.
Polyomaviridae (e.g. murine polyomavirus, SV40) are extensively studied DNA tumor viruses and have served as models for icosahedral capsid assembly with the crystal structure of both viruses being known (26, 27). Polyomavirus assembly occurs in a series of discrete steps, with 5 capsid proteins (VP1) forming a capsomere and 72 capsomeres forming the capsid (7d symmetry).

2. MATERIALS AND METHODS

2.1. Purification of virus-like particles (VLPs)

The gene encoding the major capsid protein of muPy was cloned into pENTR baculo expression vector (Invitrogen) and was expressed in Sf9 insect cells. VP1readily formed capsids not distinguishable from native virus. Sf9 cells were lysed in lysis buffer (10 mM Tris, 50 mM NaCl, 0.1 mM $CaCl_2$, 0.01% Triton X-100) with moderate agitation and sonication (3x 45s cycles). The lysate was cleared by centrifugation (16000xg, 30min, 4°C) and the supernatant was layered above a 30% sucrose shelf and the VLPs were pelleted by

ultracentrifugation (100000xg, 2h, 4°C). While this step routinely yielded VLPs of 90% purity, an improvement of purity could by achieved by banding the VLPs in a CsCl gradient (150000xg, 24h, 4°C), although with a considerable loss in yield.
Where necessary, VLPs were further purified by CsCl gradient ultracentrifugation, optimized for separation of full (1.34 g/mL) and empty (1.29 g/mL) VLPs (values from (28)) in a Beckman SW 60 Ti rotor at 50000 rpm for 15h.

2.3. Preparation of gold nanoparticles

Highly monodisperse gold nanoparticles of 5nm size were produced by the method of Geuze (29) by reducing tetrachloroauric acid (HAuCl4) with sodium citrate and tannic acid. The reduction rate and therefore the size of the particles were controlled by the amount of tannic cid added. Particles were stabilized by adsorption of small quantities of BSA to the gold particles. The size distribution as well as the particle count of each batch of gold nanoparticles was analyzed by static light scattering (ZetaSizer, Malvern Instruments, UK) and by electron microscopy.

2.4. Incorporation of gold nanoparticles into VLPs

Adding gold nanoparticles to disassembled VLPs before initiating the reassembly reaction lead to the incorporation of 1-3 gold nanoparticle into the capsid. To disassemble capsids into capsomeres, VLPs were dialyzed against disassembly buffer (50mM Tris-Cl, 150mM NaCl, 1mM EGTA, 20mM DTT; pH 7.4) for 2h at room temperature using a dialysis membrane with 10.000 MWCO (Pierce). The disassembled VLPs were mixed with gold nanoparticles at varying ratios and re-assembly was initiated by dialysis in re-assembly buffer (50mM Tris-Cl, 150mM NaCl, 5mM $CaCl_2$, 1% DMSO) for 18h at room temperature.

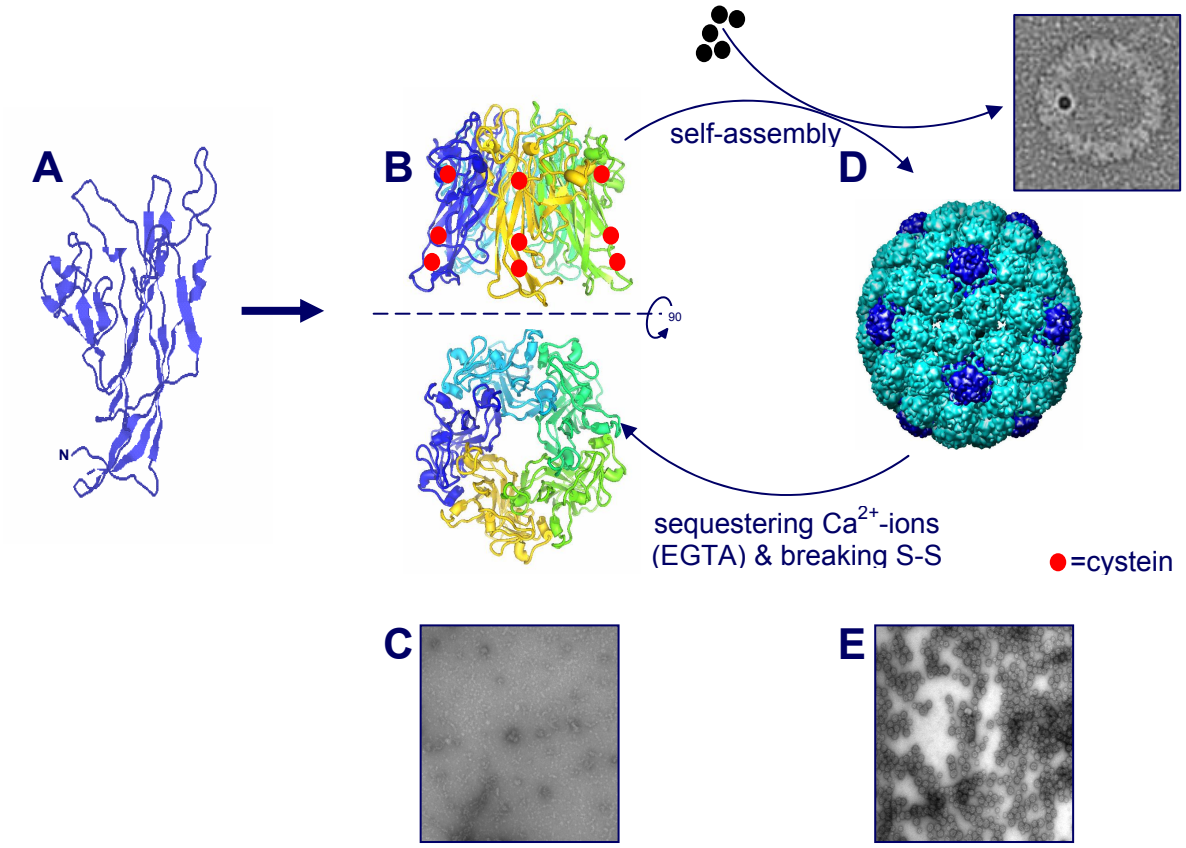

Fig. 1: Schematic representation of the packaging process. 5 VP1 proteins (A) form a capsomere (B,C) and 72 capsomeres form the capsid (D, E). The capsid is held together by Ca2+-bridges and disulfide bonds and can

reversibly be switched between capsomere and capsid conformation *in vitro* by altering the buffer conditions. Adding a payload to disassembled capsomeres prior to assembly leads to the packaging of the payload.

2.5. Electron microscopy

VLPs were spotted onto formvar-coated copper grids (ProSciTech) and negatively stained with 2% uranyl acetate to enhance the contrast. They were imaged with a Jeol electron microscope with beam strength of 80 keV at 120.000 x magnification.
Cells were fixed with 8% PFA in 0.1 M phosphate buffer, pH 7.35, for 2 h at room temperature. They were then processed for frozen sectioning and sections retrieved using methylcellulose/sucrose as described previously (30).

2.6. Computer tomographic reconstruction of gold-incorporating VLPs.

A tilting electron microscope (JEOL F30) was used to obtain image series of single gold-packaged VLPs at angles from +60 to -60 degrees to obtain a three-dimensional reconstruction of the VLPs to prove the actual position of the gold nanoparticle in relation to the VLP. EM tomography showed that gold nanoparticles are neither incorporated in the hollow capsid nor do they unspecifically decorate the inner or outer surface of the capsid shell, but are actually incorporated in the capsid replacing a similar sized capsomere.
The likely mechanism by which gold nanoparticles are incorporated into the capsid shell is sulfide linkage between the gold and cysteines 83 and 242 of the capsomere arm (Figure 1). During assembly, the cysteines form intercapsomeric disulfide bonds to stabilize the capsid (12). By forming a sulfide link between one or more capsomeres and gold nanoparticles, the nucleation process necessary for capsid assembly (8) is initiated.

2.7. Surface enhanced Raman spectroscopy (SERS)

All Raman spectra were collected using an RM1000 (G97005) Raman system (Renishaw, Gloucestershire, UK). Excitation was achieved using a 785 nm high-performance near-IR (HPNIR) diode laser (Renishaw), focused through a ×50 objective (N PLAN L long working distance, Leica, Milton Keynes, UK) and filtered to give ~10 mW total laser energy at the sample. Spectra were collected in static mode over the range 1260 cm^{-1} to 1800 cm^{-1} with a 40-second scan time and 10 repeats. Wavenumber calibration was carried out using the 520.5 cm^{-1} line of a silicon wafer. A spectral resolution of about 2.3 cm^{-1} was used.

2.8. *In-vitro* transduction of cells with hybrids

Approximately $5x10^5$ cells of fibroblast cell line NIH-3T3 were seeded onto microscope cover slips placed in six-well culture dishes and allowed to attach to the glass at 37°C with 5% CO_2 in humid atmosphere over night in 2ml DMEM supplemented with 10% fetal calf serum and glutamine. Cells were washed three times with PBS and then overlaid with 800μl OptiMEM (Invitrogen). 10μl of hybrid VLPs were added to the media and incubated for 3h. Cells were fixed with and used for electron microscopy.

3. RESULTS

3.1. Purification of VLPs

The purity of muPy VLPs from insect cells was analyzed by SDS-PAGE gel electrophoresis followed by coomassie protein stain or specific detection of muPy VP1 with protein or virion specific antibodies (kindly provided by Prof Consigli (10)) to check for impurities and by electron microscopy to check the integrity of the VLPs obtained (Figure 1 E). 85%-90% purity of VLPs was routinely achieved by just using the sucrose shelf. While CsCl gradient ultracentrifugation improved purity up to 95%, it incurred a dramatic loss in yield (up to 50%). We therefore settled with the sucrose shelf method, as experimentation indicated that the remaining impurities did not affect dis- or subsequent reassembly.

3.2. Incorporation of gold nanoparticles in VLPs

Previous experiments with proteins suggested a high packaging capacity for the VLPs (data not shown). Initial EM images looked promising, with gold nanoparticles associated with the capsids.

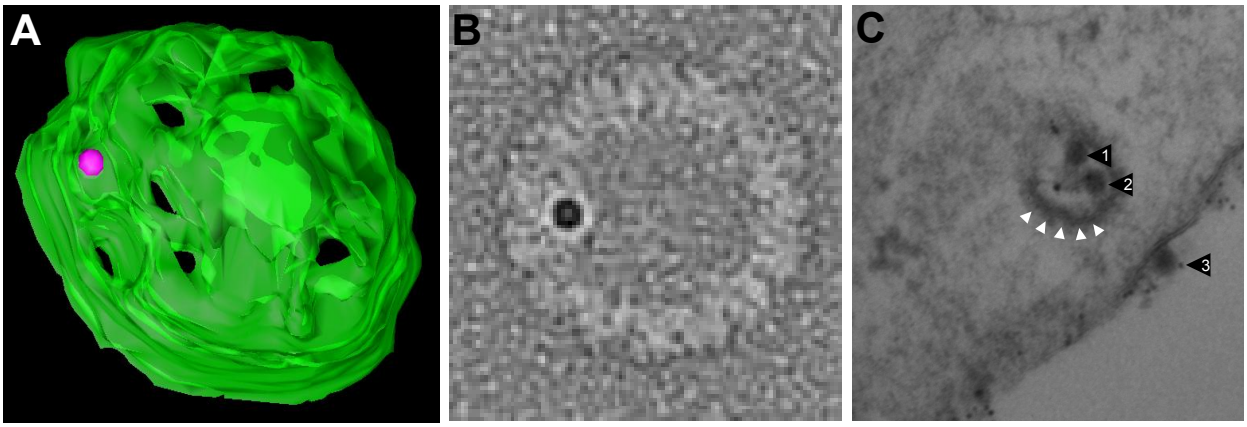

Fig. 2: Electron microscopic image **(A)** and computational reconstruction after EM tilt series **(B)** of a 5nm gold nanoparticle incorporated into the capsid shell of a muPy VLP. While normal TEM (inset) cannot differentiate between gold nanoparticles co-localized or unspecifically attached to VLPs, TEM tomography with the help of computer-aided reconstruction, can create a 3-dimensional image of the VLP. This shows clearly that the gold nanoparticle (pink) is neither fully on the outside nor inside of the capsid, but occupies the place of a capsomere, sitting right in the capsid shell. **(C)** VLPs retain their capacity to enter susceptible cell lines (NIH-3T3) after gold incorporation and can be detected inside cells by EM. Dotted white line indicates the cell surface. Black arrows indicate 3 VLPs: VLP 1+2 are taken up by a cellular organelle, most likely a caveolae. The white arrows indicate the organelle membrane. VLP 1 does not contain a visible gold nanoparticle, while VLP 2 does. VLP 3 has just attached to the cell membrane.

Although, from normal EM images, it was impossible to tell whether the gold nanoparticles were tightly associated with the VLPs or just lying above or below the VLPs during the imaging. Therefore, we used the EM to obtain a tilt series of images from one sample. With this technique, the sample holder inside the electron microscope is tilted from -60° to +60°, taking an image of the same object at every degree. With the help of computer reconstruction (31), a tilt series is then used to construct a three-dimensional representation of the object as can be seen in Figure 2 A+B.

The computer reconstruction clearly shows that the gold nanoparticles are not loosely associated with the VLPs but tightly integrated into the capsid shell, thereby replacing one capsomere.

While the initial results with gold incorporation were rather poor, we optimized the reaction by varying the ratios of gold nanoparticles to capsomeres (Figure 3). These results show that mainly the concentration of gold nanoparticles is responsible for a good packaging efficiency. Simply increasing the protein concentration with few gold nanoparticles available does not improve the efficiency. In contrast, at higher gold nanoparticle concentrations, a good packaging efficiency can be obtained even at low to intermediate protein concentrations.

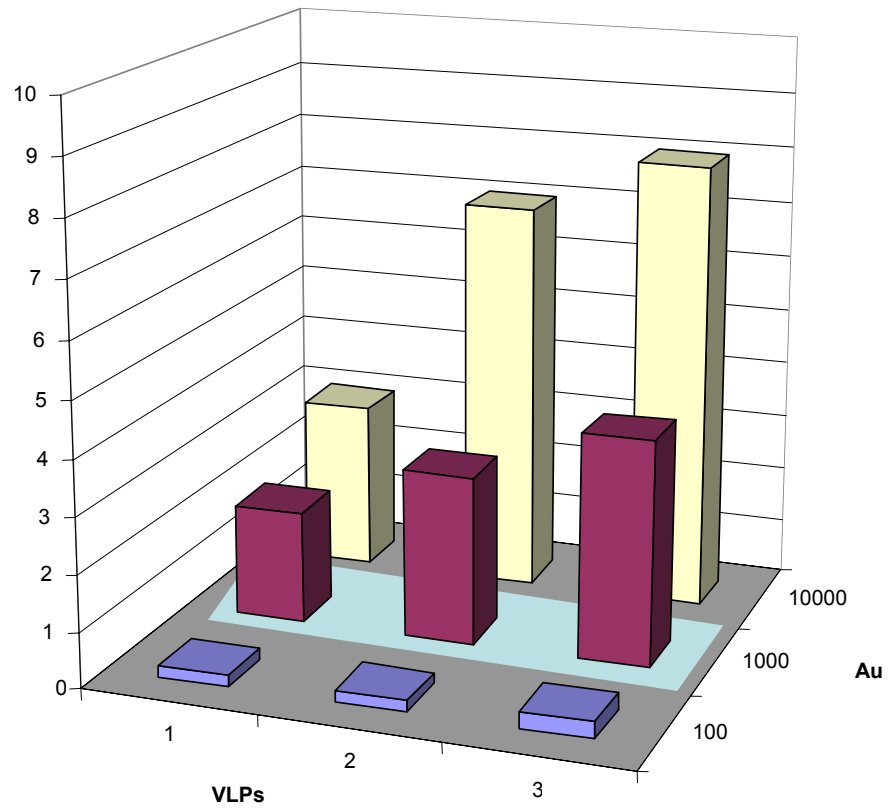

Fig. 3: The incorporation efficiency of gold nanoparticles depends on the gold concentration, but is only slightly influenced by the VLP concentration, with higher gold concentration leading to as much as 80% of VLPs incorporating one or more nanoparticles.

3.3. Gold nanoparticles are coordinated by cysteines

To find out how the gold nanoparticles are incorporated into the VLPs, we purified hybrids after the re-assembly reaction by ultracentrifugation in a CsCl gradient (Figure 3). Fractions were collected and probed with virion-specific antisera against muPy VLPs and with silver-enhancement staining against gold nanoparticles. The fractions that reacted strongest with both antisera and silver enhancement were then treated with DTT and imidazole, respectively. DTT will reduce disulfide bonds (or sulfide-gold-bonds), while imidazole will break interactions between metals and histidines. The treated hybrids were then centrifuged again and the resulting pellets and supernatants were probed again for VP1 and gold reactivity.

After imidazole treatment, both the VP1 and gold reactivity was found in the supernatant. In contrast, after DTT treatment, the VP1 reactivity was found in the supernatant, while the gold nanoparticles were found in the pellet.

We conclude that the separation of VP1 and gold reactivity after DTT treatment, but not after imidazole treatment, shows that the incorporation of the gold nanoparticles in mediated by disulfide bonds between the cysteines in the VP1 capsomeres and the molecular gold.

This interpretation is strengthened by the fact that the capsomeres in the intact capsid interlink via cysteine-mediated disulfide bonds as well (12) and that the gold nanoparticles seem to be intercalated into the capsid shell and not associated ith the outside or inside surface.

Preliminary data (not shown) indicated that there is size optimum for gold nanoparticles to be incorporated into VLPs from 5-7nm. This size range corresponds to the size of capsomeres as measured by light scattering. This coincidence also argues in favor of a cysteine-mediated coordination of gold-nanoparticles being build into the capsid instead of a capsomere.

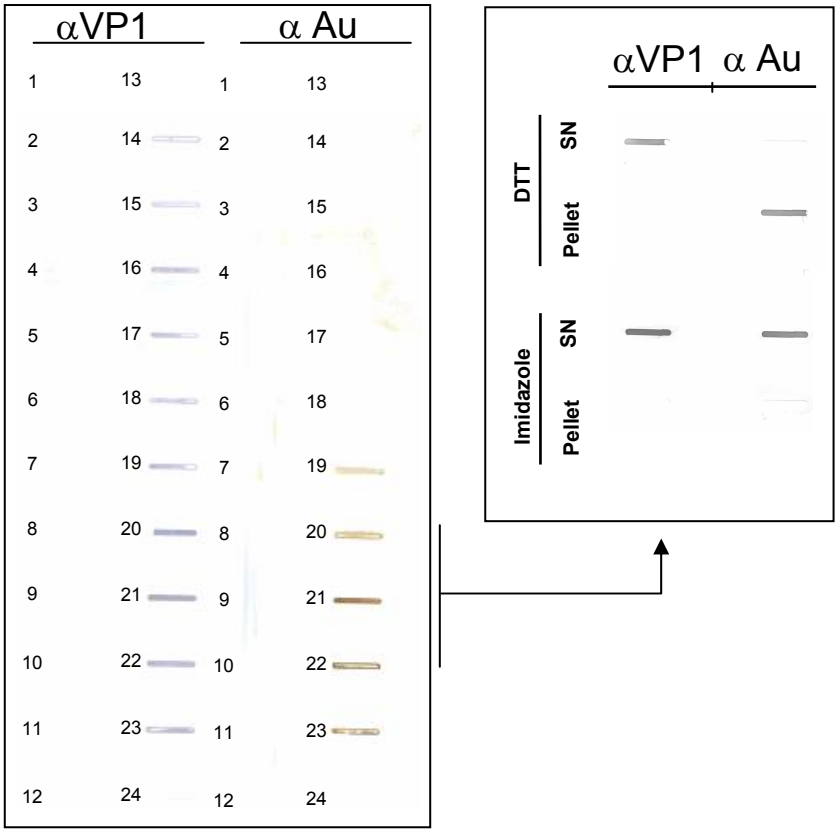

Fig. 4: Capsomeres link which each other via disulfide bonds (Figure 1) to form the capsid. The cysteines normally participating in these disulfide bonds strongly bind to the gold. To prove the binding of cysteines to the gold, VLPAu were purified, protease-digested and then treated with imidazole or DTT. While imidazole neutralizes the metal-binding capacity of histidines, DTT breaks the sulfide bonds. When centrifuged again, gold nanoparticles still attached to VLPs remain in the SN, while free gold nanoparticles will be pelleted.

3.4. Hybrids are able to enter cells normally

To utilize the full potential of these new organic-inorganic hybrids for various forms of applications as discussed further below, cellular uptake would be desirable. To test for cellular uptake, NIH-3T3 cells known to be susceptible for muPy were incubated with hybrid VLPs and analyzed by electron microscopy after hybrids were allowed to be internalized. Figure 2 C shows a representative EM image of a cell after uptake of hybrid VLPs. It is noteworthy that VLPs, even with incorporated gold nanoparticles are taken up into cellular organelle as normal VLPs would. One has to note that this image was taken with hybrid VLPs before the optimal reaction ratio (Figure 4) had been determined.

3.5. Surface-enhanced Raman spectroscopy of assembled and disassembled VLPs

One of our main goals is deciphering the cues, conditions and conformational changes responsible for viral dis- and reassembly. Raman spectroscopy is a very powerful technique to probe structure and conformational changes in molecules, although it has only seldomly been applied to such large macromolecules as viruses (20-25). Another big advantage of Raman spectroscopy is its insensitivity to water, making it possible to probe molecules in solution. The enhancement effect of silver and gold colloids is known for a long time, so we thought to use surface-enhanced Raman spectroscopy (SERS) to probe our hybrid VLPs.

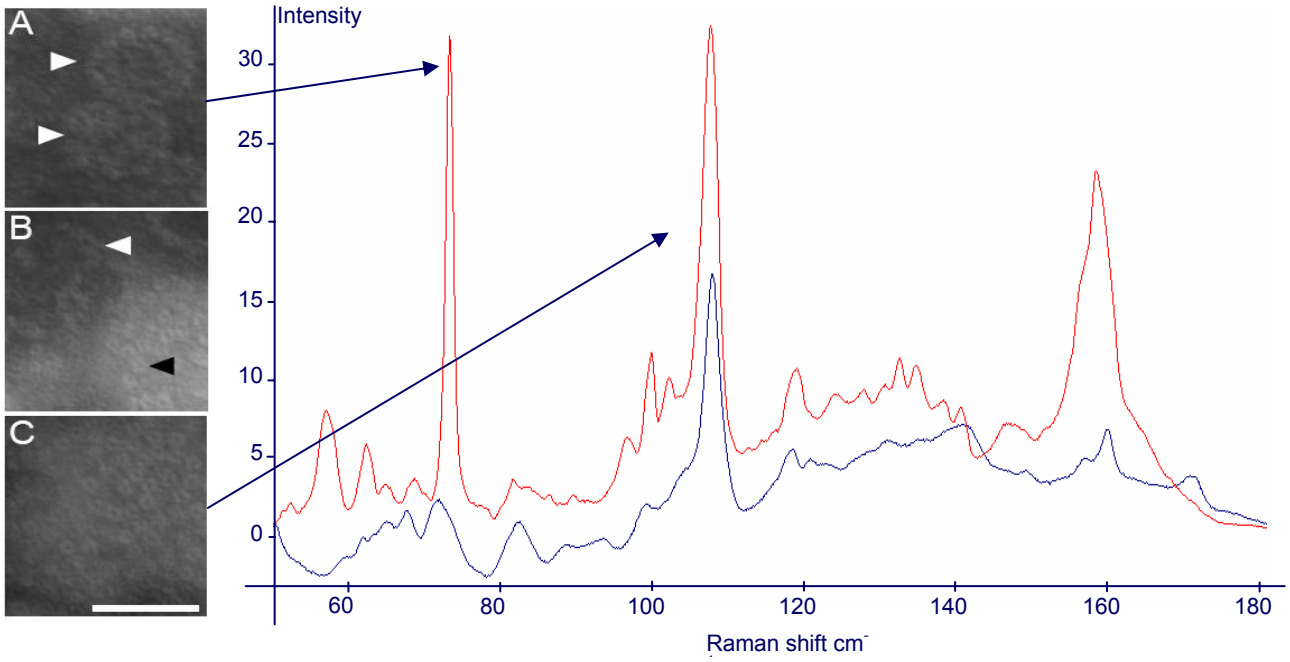

Fig. 5: Assembled **(A)** and disassembled VLPs **(C)** show distinct Raman spectra *in vitro*. EGTA and DTT, necessary for disassembly, do not produce a Raman signal at the concentrations used. **(B)** shows an disassembly intermediate, where some capsids a still (partially) assembled, while others have already dissolved into capsomeres. This intermediate structure only appears briefly and no Raman spectrum could be recorded. White arrows indicate capsids and the black arrow indicates capsomeres.

As a prove-of-concept (Figure 5), we recorded SERS spectra of assembled (Figure 5 A) and disassembled VLPs (Figure 5 C) mixed with gold nanoparticles *in vitro*. As can be seen in Figure 5, we were able to obtain two distinct spectra for assembled and disassembled VLPs. Overall, the spectra for both forms can be reproduced with high accuracy and both spectra have the same general form, indicated minor conformational changes during disassembly.

It has been recently shown that it is possible to obtain SERS spectra from intracellular gold nanoparticles (32). In future experiments we will therefore aim to combine the techniques pioneered here to obtained SERS spectra of (dis-)assembly intermediates from internalized VLPs *in vivo*.

4. DISCUSSION

The controlled dis- and re-assembly of icosahedral viruses has been demonstrated repeatedly in the literature and exploited to transfer different therapeutics into cells (4, 5). Here we show the controlled incorporation of inorganic gold nanoparticles into the capsid shell of murine polyomavirus virus-like particles. The number of incorporated gold particles can be controlled during the assembly process by varying the ratio of capsomeres to gold nanoparticles. Our preliminary analysis shows that the coordinated incorporation of gold nanoparticles is mediated by covalent sulfide bonds between the capsid proteins cysteine residues and the molecular gold. The incorporation of gold nanoparticles into the capsids does not interfere with the VLPs ability to enter susceptible cell. The hybrids are clearly recognizable in EM images of transduced cells and enable many interesting follow-up applications.

The most apparent technique is the use of the hybrid particles to track virus movement from the cell surface into the cytoplasm during infection. The special properties of gold enable the tracking of the hybrids by fluorescent and diffraction light microscopy as well as electron microscopy. Especially electron microscopy will allow to obtain images of unprecedented resolution especially of the disassembly process. The covalent attachment of the gold with the capsid shell allows to track the otherwise dissolving capsid during the disassembly process. The incorporation of the gold into the capsid leaves the inner cavity free to transport a

payload for simultaneous therapy and imaging. In addition, the presence of the gold itself can be used therapeutically.

In hyperthermal therapy, laser or microwave radiation directed to internalized metal particles is used to locally heat up the particles and kill the surrounding tissue.

Another application of the hybrids is their use in nanochemical or nanoelectronical devices. Bacteriophages have recently been utilized as organic templates to construct metal nanowires. These nanowires were used as electrodes in batteries (6, 7). Our current research focuses on the strong enhancement effect of gold nanoparticles in Raman spectroscopy. We showed in this report that surface-enhanced Raman spectroscopy (SERS) can be used to differentiate between assembled and disassembled capsids (Figure 5). With the ability of hybrid particles to transduce living cells, we hope to obtain SERS spectra from internalized VLPs, gaining information on *in vivo* disassembly.

REFERENCES

1. Leavitt, A. D., Roberts, T. M. & Garcea, R. L. (1985) *J Biol Chem* **260,** 12803-9.
2. An, K., Gillock, E. T., Sweat, J. A., Reeves, W. M. & Consigli, R. A. (1999) *J Gen Virol* **80 (Pt 4),** 1009-16.
3. Salunke, D. M., Caspar, D. L. & Garcea, R. L. (1986) *Cell* **46,** 895-904.
4. Braun, H., Boller, K., Lower, J., Bertling, W. M. & Zimmer, A. (1999) *Biotechnol Appl Biochem* **29 (Pt 1),** 31-43.
5. Forstova, J., Krauzewicz, N., Sandig, V., Elliott, J., Palkova, Z., Strauss, M. & Griffin, B. E. (1995) *Hum Gene Ther* **6,** 297-306.
6. Nam, K. T., Kim, D. W., Yoo, P. J., Chiang, C. Y., Meethong, N., Hammond, P. T., Chiang, Y. M. & Belcher, A. M. (2006) *Science* **312,** 885-8.
7. Mao, C., Solis, D. J., Reiss, B. D., Kottmann, S. T., Sweeney, R. Y., Hayhurst, A., Georgiou, G., Iverson, B. & Belcher, A. M. (2004) *Science* **303,** 213-7.
8. Friedmann, T., Doolittle, R. & Walter, G. (1978) *Nature* **274,** 291-293.
9. Sasnauskas, K., Buzaite, O., Vogel, F., Jandrig, B., Razanskas, R., Staniulis, J., Scherneck, S., Kruger, D. H. & Ulrich, R. (1999) *Biological Chemistry* **380,** 381-386.
10. Gillock, E. T., Rottinghaus, S., Chang, D., Cai, X., Smiley, S. A., An, K. & Consigli, R. A. (1997) *J Virol* **71,** 2857-65.
11. Buck, C. B., Pastrana, D. V., Lowy, D. R. & Schiller, J. T. (2004) *J Virol* **78,** 751-7.
12. Brady, J. N., Winston, V. D. & Consigli, R. A. (1977) *J Virol* **23,** 717-24.
13. Pattenden, L. K., Middelberg, A. P., Niebert, M. & Lipin, D. I. (2005) *Trends Biotechnol* **23,** 523-9.
14. Goldmann, C., Stolte, N., Nisslein, T., Hunsmann, G., Luke, W. & Petry, H. (2000) *J Virol Methods* **90,** 85-90.
15. Zhang, S. (2003) *Nat Biotechnol* **21,** 1171-8.
16. Tseng, R., Tsai, C., Ma, L., Ouyang, J., Ozkan, C. & YANG, Y. (2006) *Nature Nanotechnology* **1,** 72-77.
17. Frazer, I. H., Quinn, M., Nicklin, J. L., Tan, J., Perrin, L. C., Ng, P., O'Connor, V. M., White, O., Wendt, N., Martin, J., Crowley, J. M., Edwards, S. J., McKenzie, A. W., Mitchell, S. V., Maher, D. W., Pearse, M. J. & Basser, R. L. (2004) *Vaccine* **23,** 172-81.
18. Cavazzana-Calvo, M., Hacein-Bey, S., de Saint Basile, G., Gross, F., Yvon, E., Nusbaum, P., Selz, F., Hue, C., Certain, S., Casanova, J. L., Bousso, P., Deist, F. L. & Fischer, A. (2000) *Science* **288,** 669-72.
19. Li, H. & Thomas, G. (1991) *J Am Chem Soc* **113,** 456-462.
20. Rodriguez-Casado, A., Moore, S. D., Prevelige, P. E., Jr. & Thomas, G. J., Jr. (2001) *Biochemistry* **40,** 13583-91.
21. Rodriguez-Casado, A. & Thomas, G. J., Jr. (2003) *Biochemistry* **42,** 3437-45.
22. Tsuboi, M., Benevides, J. M., Bondre, P. & Thomas, G. J., Jr. (2005) *Biochemistry* **44,** 4861-9.
23. Tsuboi, M., Kubo, Y., Ikeda, T., Overman, S. A., Osman, O. & Thomas, G. J., Jr. (2003) *Biochemistry* **42,** 940-50.
24. Tsuboi, M., Overman, S. A., Nakamura, K., Rodriguez-Casado, A. & Thomas, G. J., Jr. (2003) *Biophys J* **84,** 1969-76.
25. Benevides, J. M., Bondre, P., Duda, R. L., Hendrix, R. W. & Thomas, G. J., Jr. (2004) *Biochemistry* **43,** 5428-36.

26. Liddington, R. C., Yan, Y., Moulai, J., Sahli, R., Benjamin, T. L. & Harrison, S. C. (1991) *Nature* **354,** 278-84.
27. Yan, Y., Stehle, T., Liddington, R. C., Zhao, H. & Harrison, S. C. (1996) *Structure* **4,** 157-64.
28. Kosukegawa, A., Arisaka, F., Takayama, M., Yajima, H., Kaidow, A. & Handa, H. (1996) *Biochim Biophys Acta* **1290,** 37-45.
29. Slot, J. W. & Geuze, H. J. (1985) *Eur J Cell Biol* **38,** 87-93.
30. Liou, W. W. & Goshgarian, H. G. (1997) *Exp Neurol* **145,** 258-67.
31. Kremer, J., Mastronarde, D. & McIntosh, J. (1996) *J. Struct. Biol.* **116,** 71-76.
32. Kneipp, J., Kneipp, H., Rice, W. L. & Kneipp, K. (2005) *Anal Chem* **77,** 2381-5.